ACS APPLIED BIO MATERIALS

www.acsabm.org Article

Photothermal-Induced Electrochemical Interfacial Region Regulation Enables Signal Amplification for Dual-Mode Detection of Ovarian Cancer Biomarkers

Shupei Zhang, Huizhu Ren, Hong Dai,* Liang Lv, and Yanyu Lin

Cite This: https://doi.org/10.1021/acsabm.1c00665 Read Online

ACCESS | Metrics & More | Article Recommendations | Supporting Information

ABSTRACT: Detection sensitivity of an electrochemical immunosensor mainly depends on the accessible distance toward the sensing interface; regulating the electrochemical interfacial region thereon is an effective strategy for signal amplification. Herein, a photothermal-regulated sensing interface was designed based on a near-infrared (NIR)-responsive hydrogel probe for ultrasensitive detection of human epididymis protein 4 (HE4). Silver nanoparticle-deposited graphene oxide nanosheet (AgNPs@GO) hybrids as electrochemical signal tags and a photothermal transducer, which were encapsulated in the poly(*N*-isopropylacrylamide) (pNIPAM) hydrogel, were used to develop the NIR-responsive GO@AgNPs-pNIPAM hydrogel probe. Under NIR light irradiation, the excellent photothermal effect of AgNPs@GO hybrids not only rapidly converted NIR light into heat for temperature readout but also triggered the shrinkage behavior of the hydrogel for electrochemical signal amplification. Compared with the conventional sandwich immunoassay, the shrinkage behavior of the hydrogel signal probe endowed itself with interface regulation capability to improve the electrochemical reaction efficiency; on the basis of ensuring the extended outer Helmholtz plane (OHP) region, the proposed photothermal-induced interface regulation also shortened the OHP, leading to higher sensitivity. Moreover, the obtained dual-mode signals provided satisfactory accuracy for the detection of tumor markers. Therefore, this detection scheme provided an opportunity for the broad applications of the photothermal effect in clinical diagnosis.

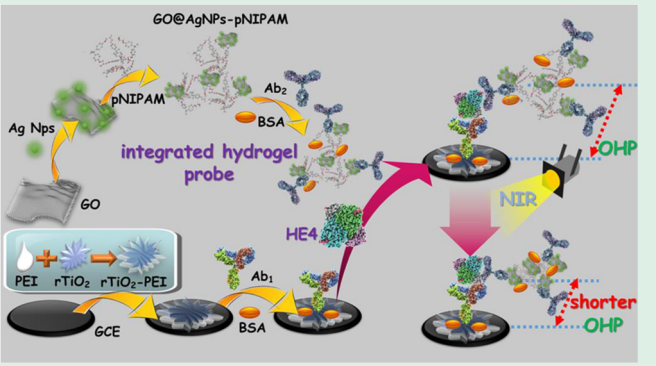

KEYWORDS: *dual mode, photothermal, near-infrared-responsive hydrogel, biosensor, ovarian cancer biomarker*

1. INTRODUCTION

Tumor markers are regarded as the objective indicator to evaluate pathogenesis and assess therapeutic effectiveness.[1,2] Therefore, the determination of low abundant tumor markers is vital for early cancer diagnosis to improve the survival rate of patients. To date, an immunoassay has been a predominant analytical method in the early diagnosis of tumor markers, which relies on the strict recognition between antigens and antibodies to ensure detection specificity.[3,4] Recently, various immunoassays have been developed for the detection of tumor markers, including fluorescence,[5] chemiluminescence,[6] electrochemiluminescence,[7] photoelectrochemical,[8] etc. Among them, electrochemical immunosensors have attracted substantial attention benefiting from their high sensitivity, fast response, simple setup, and easy miniaturization.[9,10] To further improve the analytical performance of an immunosensor, it is of paramount importance for developing an effective signal amplification strategy to meet the demand of high sensitivity in clinical diagnosis.

As a matter of fact, sensitivity is particularly restricted by the accessible distance between signal labels and the sensing interface, which is a great challenge in electrochemical immunosensors.[11,12] Generally, the electrochemical response only occurs when the electrochemically active material is in the vicinity of the outer Helmholtz plane (OHP), thereby the signal labels within the OHP are "effective" to generate the intense electrochemical signal.[13,14] Therefore, increasing the loading amount of signal labels and regulating the OHP region of the sensing interface are essential for signal amplification. Presently, the mainstream reports are mainly focused on developing a "Faraday cage"-type immunoassay, using two-dimensional graphene oxide (GO) nanosheets as carriers to enhance the signal amount and extend the OHP region.[15,16] In this state, GO nanosheets overlap on the electrode surface to

Received: June 6, 2021
Accepted: July 26, 2021

https://doi.org/10.1021/acsabm.1c00665
ACS Appl. Bio Mater. XXXX, XXX, XXX−XXX

form a ringed Faraday cage, where signal labels could directly involve in the electrochemical reaction and allow the electrons to freely transfer to the electrode interface.[17,18] Nevertheless, the distance between signal labels and the electrode surface is finite in the Faraday cage; thus, the OHP region is fixed and exhibits limited signal amplification. On this basis, an intelligent signal probe with interface regulation capability to shorten the OHP can circumvent these difficulties, resulting in the improved accessibility of the sensing interface and increased loading amounts of signal tags to realize further signal amplification.

Considering that the phase transition behavior of the near-infrared (NIR)-responsive hydrogel is a promising tool to regulate the sensing interface,[19,20] an intelligent NIR-responsive hydrogel probe was well designed by incorporation of photothermal silver nanoparticles/GO nanosheet (GO@AgNPs) hybrids into the thermosensitive poly(*N*-isopropylacrylamide) (pNIPAM) hydrogel matrix, wherein GO@AgNP hybrids acted not only as a thermal converter by virtue of the outstanding photothermal effect but also as electrochemical signal tags due to the inherent electroactivity of AgNPs.[21,22] In this regard, the obtained GO@AgNPs-pNIPAM hydrogel probe with a three-dimensional (3D) cross-linked network was suitable as a container to load substantial signal tags, endowing hydrogel with shrinkage behavior to regulate the sensing interface. Under NIR light irradiation, GO@AgNP hybrids rapidly increased the electrode surface temperature by light-to-heat conversion until the volume phase transition temperature (VPTT) was exceeded, resulting in the shrinkage behavior of the hydrogel to reduce the distance between adjacent signal tags.[23,24] Furthermore, the shrinking hydrogel shortened the OHP region of the electrode; thus, more AgNPs were significantly effective where they were close to the OHP and participated in the electrochemical reaction to produce the enhanced signal.[18,25] On the other hand, the generated heat on the electrode surface could be accurately and quantitatively monitored by an ordinary thermometer for temperature readout. Therefore, the GO@AgNPs-pNIPAM signal probe not only enabled accurate quantification of the target by the amplified electrochemical signal but also validated the feasibility of temperature sensing with simple equipment; the obtained dual-signal results could be mutually verified and provide more reliable sensing performance. To date, shortening the OHP region of the sensing interface to realize signal amplification and combining the dual-mode immunoassay have not been reported.

In this work, the electrochemical-interface-regulated immunoassay was first constructed by photothermal controlling to shorten the OHP region and enhance the signal, realizing electrochemical and temperature dual-signal readout for tumor marker detection. As shown in Scheme 1, using human epididymis protein 4 (HE4) as the model target and following the sandwich protocol, rutile titanium dioxide ($rTiO_2$) modified with polyethylenimine (PEI) served as the sensing substrate, which provided abundant sites for antibody immobilization and then captured the target. Subsequently, the GO@AgNPs-pNIPAM hydrogel probe with high loading capacity allowed the effective electrochemical reduction of AgNPs to generate an intense signal. Under NIR laser irradiation, the hydrogel probe was utilized as an amplifier to enhance the electrochemical signal by shortening the OHP, as well as the photothermal transducer rapidly converted the light energy into heat for temperature readout. Therefore, the proposed immunoassay with interface regulation capacity exhibits high sensitivity and accuracy for HE4 determination, which also provided new perspectives for photothermal-effect-induced signal amplification in the immunoassay.

Scheme 1. Schematic Illustration of the Fabrication of the Dual-Mode Immunoassay

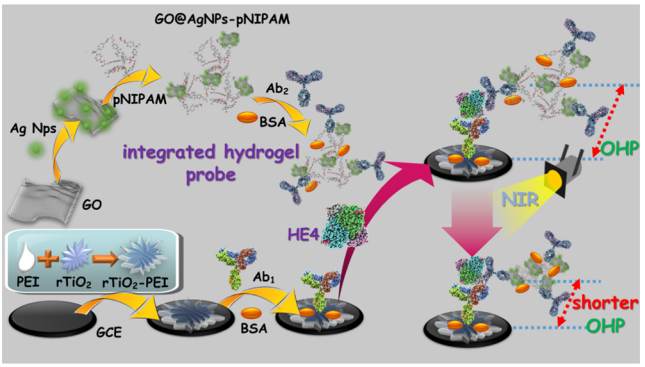

2. EXPERIMENTAL SECTION

The information about materials, reagents, and apparatus is listed in the Supporting Information.

2.1. Preparation of the $rTiO_2$-PEI Nanocomposite. $rTiO_2$ was synthesized according to a previous report with appropriate modification.[26] Subsequently, 1 mL of the PEI aqueous solution (1 wt %) was added into 1 mL of the $rTiO_2$ dispersion solution (1 mg/mL) under continuous stirring for 4 h at room temperature. After that, the suspension was centrifuged at 6000 rpm and then washed with ultrapure water three times to remove the excess PEI. Finally, the obtained $rTiO_2$-PEI product was dried and redispered in 1 mL of ultrapure water for further use.

2.2. Preparation of GO@AgNP Hybrids. Typically, GO nanosheets were synthesized using the modified Hummers' method.[27] GO@AgNP hybrids were prepared by in situ reducing Ag^+ on the GO nanosheet surface. Briefly, 500 μL of the $AgNO_3$ aqueous solution (0.01 M) was thoroughly mixed with 1 mL of the GO dispersion solution (5 mg/mL). The $NaBH_4$ aqueous solution (0.1 M, 200 μL) was added dropwise under vigorous stirring, and then the reaction mixture was constantly stirred at room temperature for 6 h. Finally, GO@AgNP hybrids were collected by centrifugation, washed with ultrapure water, and dried under vacuum overnight.

2.3. Preparation of the Multifunctional Hydrogel Probe. The GO@AgNPs-pNIPAM hydrogel was synthesized according to a previous report with slight modification.[19,28] NIPAm (10.54 mg) as a monomer, BIS (1.703 mg) as a cross-linker, and acrylic acid (AAc) (2.812 mg) as a carboxyl source were fully dissolved in ultrapure water (20 mL) under stirring, and then GO@AgNP hybrids were added and dispersed shortly through ultrasonication for 30 min. The resulting dispersion was purged with N_2 gas for 1 h. Subsequently, the APS solution as an initiator (5 mg/mL) was added into the above solution by bubbling N_2 gas for 30 min. After that, tetramethylethylenediamine (TEMED, 20 μL) as the accelerator was slowly added dropwise and polymerized for 4 h. The product was purified by centrifugation and washed to remove residual monomers and reagents. The synthesized GO@AgNPs-pNIPAM was redispersed in ultrapure water (1 mL) and treated with 200 μL of a 1-ethyl-3-(3-dimethylaminopropyl)carbodiimide (EDC) and *N*-hydroxysuccinimide (NHS) mixture solution (molar ratio: 4:1) for 1 h at room temperature. The Ab_2 solution (10 ng/mL, 500 μL) was added into the above composite and incubated for another 40 min at 4 °C. Finally, 100 μL of bovine serum albumin (BSA, 1%) was introduced into the above composite to block nonspecific binding sites. After carefully washing, the multifunctional hydrogel probe was obtained and stored in a refrigerator for further use.

https://doi.org/10.1021/acsabm.1c00665
ACS Appl. Bio Mater. XXXX, XXX, XXX−XXX

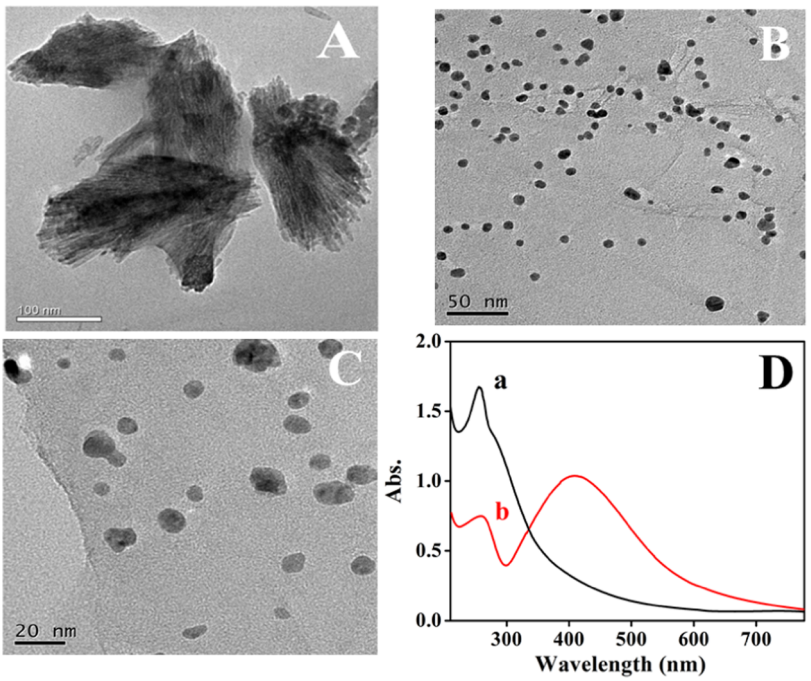

Figure 1. TEM images of (A) $rTiO_2$, (B) AgNPs@GO, and (C) AgNPs. (D) UV−vis spectra of (a) GO and (b) AgNPs@GO.

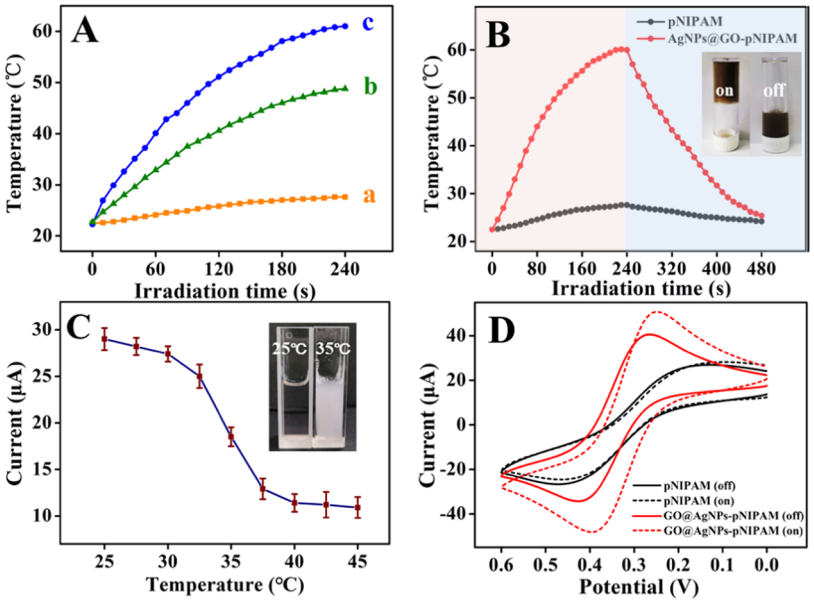

Figure 2. (A) Photothermal profiles of (a) H_2O, (b) GO dispersion, and (c) AgNPs@GO dispersion. (B) Temperature variation of the pNIPAM hydrogel and AgNPs@GO-pNIPAM hydrogel under exposure to laser irradiation (1 W/cm^2) followed by laser shut off. The inset shows the photographs of the AgNPs@GO-pNIPAM hydrogel with (left) and without (right) laser irradiation. (C) The reduction peak current of 5 mM $[Fe(CN)_6]^{3-/4-}$ upon temperature variation in 0.1 M KCl. The inset shows the shrinkage behavior of the pNIPAM hydrogel at 25 °C (left) and 35 °C (right). (D) Cyclic voltammetry (CV) responses of pNIPAM/GCE and AgNPs@GO-pNIPAM/GCE before and after laser irradiation in 0.1 M KCl containing 5 mM $[Fe(CN)_6]^{3-/4-}$.

2.4. Fabrication of the Dual-Mode Immunoassay. First, a bare glassy carbon electrode (GCE) was polished with 0.3 and 0.05 μm of the Al_2O_3 powder, successively, and then thoroughly cleaned before use. Subsequently, 5 μL of the $rTiO_2$-PEI dispersion solution (3 mg/mL) was coated onto the GCE surface. After drying, 5 μL of GLD (2.5%) was dropped onto the modified electrode ($rTiO_2$-PEI/GCE) for 40 min, followed by washing with ultrapure water and drying at room temperature. Thereafter, the obtained electrode was submerged in 50 μL of the Ab_1 solution (10 ng/mL) and incubated for 40 min at 4 °C. Subsequently, the resulted electrode (Ab_1/$rTiO_2$-PEI/GCE) was blocked with BSA (1%) for 1 h to prevent nonspecific binding. After washing once, 5 μL of various concentrations of the HE4 standard solution was applied to the electrode surface and incubated for 50 min at 4 °C to obtain HE4/Ab_1/$rTiO_2$-PEI/GCE. Finally, the prepared electrode (HE4/Ab1/rTiO2-PEI/GCE) was incubated with 5 μL of the prepared multifunctional hydrogel probe solution for another 50 min at 4 °C. The modified electrode of each step (rTiO2-PEI/GCE, Ab1/rTiO2-PEI/GCE, HE4/Ab1/rTiO2-PEI/GCE, Probe/HE4/Ab1/rTiO2-PEI/GCE) was treated with was performed under thoroughly cleaning with PBS (pH 7.5) and drying at room temperature. The finished immunosensor was stored

https://doi.org/10.1021/acsabm.1c00665
ACS Appl. Bio Mater. XXXX, XXX, XXX−XXX

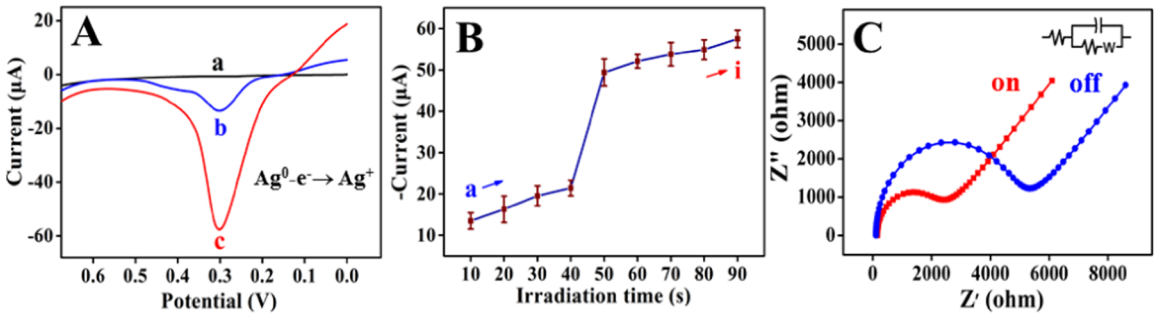

Figure 3. (A) LSV response of (a) GO-pNIPAM/GCE, (b) AgNPs@GO-pNIPAM/GCE without laser irradiation, and (c) AgNPs@GO-pNIPAM/GCE with laser irradiation (1 W/cm^2) for 40 s in 0.1 M PBS (pH 7.5). (B) The corresponding current intensity curve of AgNPs@GO-pNIPAM/GCE (a–i) with different laser irradiation times (1 W/cm^2). (C) Electrochemical impedance spectroscopy (EIS) of AgNPs@GO-pNIPAM/GCE without (blue) and with (red) laser irradiation (1 W/cm^2) for 40 s in 0.1 M KCl containing 5 mM $[Fe(CN)_6]^{3-/4-}$.

at 4 °C for the subsequent electrochemical and temperature measurements.

3. RESULTS AND DISCUSSION

3.1. Characterization of Materials. The morphology and structure of $rTiO_2$ were characterized by transmission electron microscopy (TEM) and are shown clearly in Figure 1A. $rTiO_2$ was composed of bundle-like nanosheets with an average size of about 200 nm, whose large specific area and rough surface were appropriate as the sensing substrate for the immobilization of the antibody. Figure 1B shows the TEM image of the as-prepared GO@AgNP hybrids; AgNPs were uniformly distributed on the surface of crinkled GO nanosheets, and the average diameter of AgNPs was 20 nm (Figure 1C). The results confirmed that GO nanosheets provided a large specific surface area for the loading of substantial AgNPs. Meanwhile, the UV–vis absorption spectra of the as-prepared GO and GO@AgNP hybrids are provided in Figure 1D. GO exhibited a broad absorption peak at about 252 nm (curve a), which was assigned to the π system of GO. In comparison, an extra peak of GO@AgNPs was observed at 413 nm due to the significant characteristic absorption peak of AgNPs (curve b), further revealing the good formation of AgNPs on GO.[29,30]

3.2. Photothermal Performance of Materials. The photothermal properties of the materials were evaluated by monitoring the real-time temperature. Using water as the control, 500 μL of different dispersion solutions were added into centrifuge tubes, and the temperature curves were recorded every 10 s while keeping the solution exposed to 808 nm laser irradiation with a power density of 1 W/cm^2 for 240 s. As shown in Figure 2A, the temperature of GO dispersion (curve b) evidently increased with the irradiation time due to the inherent photothermal effect of the GO nanosheet, whereas no significant temperature change was observed for water (curve a). Especially, the photothermal effect of GO@AgNPs was relatively higher than that of the single GO component, which was attributed to the surface plasmon resonance (SPR) effect of AgNPs, generating heat upon NIR irradiation efficiently and promoting the photothermal effect of the GO nanosheet. These results indicated the potential of GO@AgNPs as an effective photothermal transducer to drive the light-to-heat conversion process, which further provided the possibility to design NIR-responsive hydrogels.

As shown in Figure 2B, the NIR-responsive capability of the GO@AgNPs-pNIPAM hydrogel was also investigated by exposing it to an 808 nm laser with different irradiation times. After laser irradiation for 30 min, the original pNIPAM hydrogel (curve a) showed a negligible temperature change because the pure hydrogel has no NIR light response. In contrast, the temperature of the GO@AgNPs-pNIPAM hydrogel (curve b) rapidly increased under identical irradiation conditions, indicating its NIR-responsive capability by converting light energy into heat with high efficiency. Notably, once irradiation time exceeded 40 s, the GO@AgNPs-pNIPAM hydrogel was heated to 32 °C, which was above the VPTT of the hydrogel. As a result, the liquid GO@AgNPs-pNIPAM hydrogel quickly turned turbid until the gel state was reached (see the inset), revealing its phase transition behavior at VPTT. After the laser was shut off, the hydrogel gradually cooled back to room temperature and returned to the swollen state in a short time. Therefore, the reversible volume shrinkage of the hydrogel could be easily regulated by laser irradiation due to the excellent photothermal conversion capability of GO@AgNP hybrids.

3.3. Electrochemical Behavior of the pNIPAM Hydrogel. The temperature-dependent electrochemical behavior of the pNIPAM hydrogel was evaluated using $[Fe(CN)_6]^{3-/4-}$ as a redox probe. A plot of reduction currents of $[Fe(CN)_6]^{3-/4-}$ on the pNIPAM-modified electrode (pNIPAM/GCE) at different temperatures is given in Figure 2C; a sharp decrease in the current occurred at 32 °C and then steadily decreased as the temperature increased. This phenomenon was inferred to the fact that the pNIPAM hydrogel turned into the shrunken state at VPTT and thus blocked the diffusion of $[Fe(CN)_6]^{3-/4-}$ onto the electrode surface.[28] Clearly, the VPTT of the pNIPAM hydrogel was about 32 °C, and it can be visually observed that the shrunken pNIPAM was turbid and opaque in appearance (see the inset of Figure 2C). These results further verified that the fast electrochemical switching behavior of the sensing interface could be regulated by the phase transition of the pNIPAM hydrogel. Therefore, the pNIPAM hydrogel was especially appealing as a potential matrix and regulator for the development of the signal probe.

To further understand the photothermal modulation capability of the hydrogel for NIR-responsive stimuli, the cyclic voltammetry (CV) response was investigated under NIR light irradiation. As illustrated in Figure 2D, all of the CV curves exhibited a pair of well-defined and stable redox peaks, which were assigned to the reversible redox process of $[Fe(CN)_6]^{3-/4-}$ species on electrodes. Notably, the pure pNIPAM-modified electrode exhibited a negligible change in current intensity due to the lack of photothermal material, while the GO@AgNPs-pNIPAM hydrogel-modified electrode

https://doi.org/10.1021/acsabm.1c00665
ACS Appl. Bio Mater. XXXX, XXX, XXX–XXX

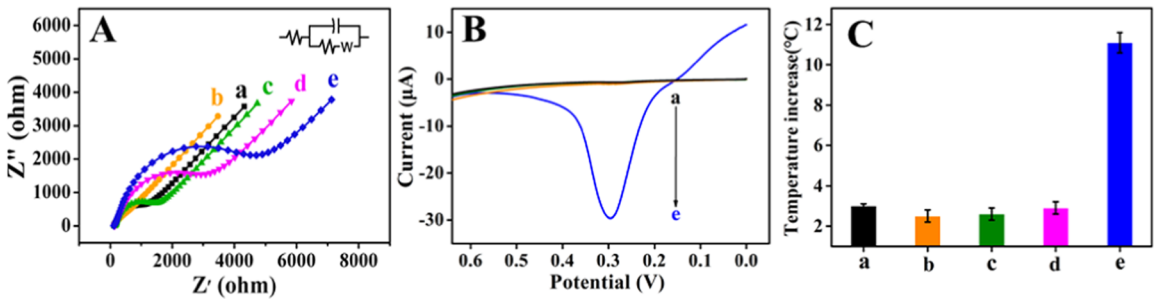

Figure 4. (A) EIS, (B) LSV responses, and (C) temperature increase of different electrodes: (a) GCE, (b) $rTiO_2$-PEI/GCE, (c) $Ab_1/rTiO_2$-PEI/GCE, (d) HE4/$Ab_1/rTiO_2$-PEI/GCE, and (e) AgNPs@GO-pNIPAM-Ab_2/HE4/$Ab_1/rTiO_2$-PEI/GCE.

displayed an obvious signal enhancement, owing to the introduction of the photothermal GO@AgNPs, which evidently improved the conductivity of the sensing interface. Especially, a significantly enhanced electrochemical response was obtained under laser irradiation. The increased current was ascribed to the laser-induced temperature increase, causing the shrinkage of the hydrogel, reducing the distance from the redox probe to the electrode surface, and facilitating the electron transfer process. In this case, the shrinkage behavior of the hydrogel made the electron transfer more effective for electrochemical signal amplification. That is, the obtained GO@AgNPs-pNIPAM hydrogel was suitable as the signal probe by simple photothermal modulation.

3.4. Signal Amplification Mechanism of the Hydrogel Probe. As illustrated by the foregoing description, the phase transition event has a drastic effect on the signal regulation of the hydrogel probe. Therefore, the pNIPAM hydrogel served as a tunable container for loading GO@AgNPs. Considering the excellent conductivity and electroactivity of AgNPs, GO@AgNPs were suitable as an inherent signal unit for electrochemical readout, wherein the intense signal was generated from the electro-oxidation process from AgNPs to Ag^+. The signal amplification effect was demonstrated by linear sweep voltammetry (LSV) and is depicted in Figure 3A; the hydrogel probe-modified electrode revealed an obvious signal due to the electrochemical oxidation of AgNPs (curve b) compared with that of the bare GCE (curve a), indicating that AgNPs possessed the high electrochemical activity. Once irradiated by the NIR laser, a significant enhancement of peak current was observed (curve c), which was ascribed to the fact that the shrunken hydrogel probe obviously compressed the sensing interface and shortened the OHP region. Therefore, the distance between adjacent AgNPs decreased, resulting in a highly effective electrochemical oxidation process and significant signal amplification.

To further illustrate the signal amplification mechanism of the hydrogel probe, a series of LSV responses under NIR laser irradiation with a time interval of 10 s were monitored (Figure 3B, curves a–i). It could be intuitively found that the peak current intensity increased from 13.5 μA (curve a) to 57.6 μA (curve i). To be specific, when the irradiation time was less than 40 s (curves a–d), the component of the pNIPAM chain was swollen and hydrophilic, hindering the active sites of the AgNP core within swollen pNIPAM and exhibiting a weak signal. Once the VPTT was reached, the current intensity was markedly enhanced and then remained constant after irradiation for 40 s (curves e–i), and the whole process was accompanied by the gradual shrink behavior of the hydrogel probe. Noticeably, more AgNPs moved closer to the electrode with an accelerated electron transfer rate, which was equivalent to shorten the OHP of the electrode. Along with the increase of the electrode temperature, a massive amount of AgNPs easily approached the OHP to involve in the electrochemical reaction and produce an intense signal. In this view, the proposed hydrogel probe served as not only a photothermal converter to induce the phase transition but also a signal amplifier in virtue of its shrinkage behavior.

Similar to the electrochemical impedance spectroscopy (EIS) experiment (Figure 3C), the electron transfer resistance (R_{ct}) significantly decreased after 40 s of irradiation (curve red) compared to that without laser irradiation (curve blue). It demonstrated that the resistance of the hydrogel probe degraded with prolonging irradiation time, as the improved conductivity of the hydrogel allowed rapid electron transport. Particularly, this evidence was consistent with the results of LSV, thereby verifying the feasibility of the NIR-responsive hydrogel in signal amplification.

3.5. Characterization of the Dual-Mode Immunosensor. EIS is a powerful method for estimating the interfacial behavior of the stepwise modification process. In Figure 4A, the $rTiO_2$-PEI-modified electrode showed smaller R_{ct} compared with the bare GCE (curve a), as the positive charge of PEI attracted the negative $[Fe(CN)_6]^{3-/4-}$ and thus effectively facilitated the electron transport rate (curve b). However, following the stepwise immobilization of Ab_1, HE_4, and the hydrogel probe via specific recognition, the resistance of the sensing interface increased gradually (curves c–e), revealing that the high steric hindrance effect of the immune conjugate greatly hindered the diffusion of redox species to the electrode interface. The above results indicated the successful construction of the dual-mode immunosensor. The fabrication procedures were also monitored by LSV signal responses and temperature variation. As shown in Figure 4B,C, in the absence of the hydrogel probe, there was no LSV signal and weak temperature variation was observed (curves a–d). Under laser irradiation, once the hydrogel probe was captured onto the sensing interface, the temperature elevation achieved the maximum and the intense LSV signal occurred (curve e), which was ascribed to the excellent photothermal conversion capability and ingenious phase transition behavior of the hydrogel probe. These results demonstrated that GO@AgNPs-pNIPAM-Ab_2 could be used as an ideal dual-mode probe to construct an immunosensor.

3.6. Optimization of Experimental Conditions. To obtain the satisfactory analytical performance of the immunosensor, some experimental conditions were optimized and are shown in Figure S1. As depicted in Figure S1A, the optimal current was obtained when the modification time of

https://doi.org/10.1021/acsabm.1c00665
ACS Appl. Bio Mater. XXXX, XXX, XXX–XXX

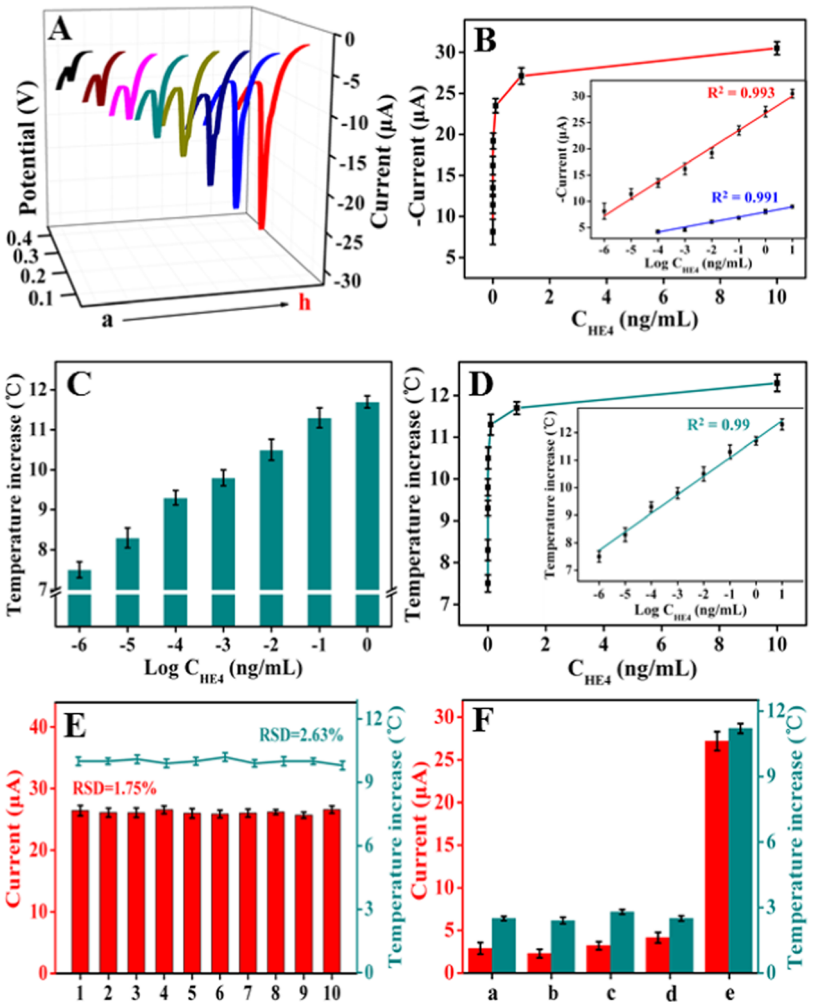

Figure 5. (A) LSV responses of the immunosensor for detecting HE4 of various concentrations 10^{-6}–10 ng/mL (a–h) under laser irradiation; (B) the corresponding calibration curves of the immunoassay with (red) and without (blue) laser irradiation; (C) temperature histograms for HE4 detection (a–h); (D) the corresponding linear relationship between temperature and the concentration of target HE4; (E) the reproducibility of the immunosensor by electrochemical detection (curve red) and photothermal detection (curve green); and (F) the selectivity of 10 ng/mL (a) AFP, (b) BSA, (c) PSA, (d) IL-6, and (e) 1 ng/mL HE4 by electrochemical detection (curve red) and photothermal detection (curve green).

PEI on $rTiO_2$ was 4 h, which was suitable to fabricate the sensing substrate. Moreover, the current intensity increased with increasing the $AgNO_3$ reduction time and the maximum signal was acquired at 40 min, indicating that the loading capacity of GO reached saturation (Figure S1B). As shown in Figure S1C, a gradual decrease in the current was observed with the immobilization time of Ab_1 and reached the minimum value at 50 min, which was chosen as the maximum immobilization capacity of the substrate. Subsequently, the peak current decreased as the recognition time of HE4 increased and then remained stable after 40 min, which was considered to be the optimal recognition time for the immunoreaction (Figure S1D). In addition, 40 min was chosen as the optimal incubation time of the hydrogel probe for the immunosensor since the signal reached the maximum and remained constant (Figure S1E). For the pH of the buffer solution, the current response increased from 5.5 to 6.5 but evidently decreased once the pH value exceeded 6.5; therefore, pH 6.5 was adopted for further experiments (Figure S1F).

3.7. Analytical Performance of the Immunoassay. Under the above optimized experimental conditions, the analytical performance of the immunosensor was investigated after the measurement of a serial concentration of HE4. As displayed in Figure 5A, the LSV current response of the immunosensor increased with the increasing concentration of HE4 (from a to h) under laser irradiation, which corresponds to the curve fitting in Figure 5B. Furthermore, a good linear relationship was obtained between the peak current intensity and the logarithm of HE4 concentration from 10^{-6} to 10 ng/mL (see the inset of Figure 5B). The equation of the curve regression fit was $I = 3.26 \lg C + 25.8$ ($R^2 = 0.993$), and the detection limit (LOD) was as low as 3.3×10^{-4} pg/mL (S/N = 3, curve red). In contrast, another standard curve without laser irradiation was established: $I = 0.968 \lg C + 7.98$ ($R^2 = 0.991$) with a LOD of 3.3×10^{-2} pg/mL (curve blue). It was obvious that this immunosensor displayed wider linear ranges and a lower detection limit for HE4 detection under laser irradiation, indicating that this kind of photothermal-induced signal amplification strategy evidently improved the sensitivity and sensing performance of the immunosensor. Meanwhile, the photothermal readout was also performed by recording the temperature increase (ΔT). As displayed in Figure 5C, the elevated temperature was positively related to the concentration of HE4. Besides, the regression equation was described

https://doi.org/10.1021/acsabm.1c00665
ACS Appl. Bio Mater. XXXX, XXX, XXX–XXX

as $\Delta T = 0.672 \lg C + 11.8$ ($R^2 = 0.990$) with a low LOD of 3.3×10^{-4} pg/mL (Figure 5D). Therefore, compared with other reported methods for HE4 detection (listed in Table S1), this work exhibited the distinct advantage of dual readout by combining the electrochemical signal with the temperature output to realize a more sensitive and persuasive analysis.

3.8. Specificity and Reproducibility of the Dual-Readout Immunosensor. It was necessary to evaluate specificity as an essential criterion for developing the immunoassay. The LSV current intensity and temperature variation after the individual addition of 1 ng/mL AFP, IL-6, PSA, BSA, and HE4 are revealed in Figure 5F. As expected, only target HE4 yields significant augmentation in both current (curve red) and temperature (curve green) responses; in contrast, the addition of interference hardly affected the detection result. It was attributed to the specific immune recognition; thus, this designed dual-readout protocol exhibited favorable selectivity for the HE4 assay. Furthermore, the reproducibility of the developed immunosensor was verified by analyzing 10 resultant electrodes incubated with 1 ng/mL HE4 for parallel experiments. As shown in Figure 5E, the relative standard deviation (RSD) of the electrochemical response was 1.75% (curve red). Also, the RSD of temperature measurement was calculated to be 2.63% (curve green), indicating the commendable reproducibility of the immunosensor. In addition, the immunosensors were stored at 4 °C and tested every day to estimate their long-term stability. The result is displayed in Figure S2; after 7 days, the electrochemical signal still remained about 95.7% of the initial value and the temperature response decay was less than 6%, indicating that the immunosensor possessed acceptable stability.

3.9. Detection of HE4 in Human Serum Samples. To demonstrate the application potential of the proposed immunosensor in practical samples, the standard addition method was used for the determination of HE4 in human serum samples. Specifically, different concentrations of HE4 were mixed with the human serum samples and analyzed by the constructed method. As shown in Table S2, the recoveries ranged from 95.8 to 101.9% by electrochemical detection, and the temperature determination was calculated to be 98.6–113.8%, revealing the prospective potential of this dual-readout immunosensor in clinical diagnosis.

4. CONCLUSIONS

In summary, a facile and universal method for signal amplification was developed by photothermal-induced electrochemical interface regulation, realizing the electrochemical and temperature dual-mode detection of ovarian cancer biomarkers. According to the presented results, this kind of signal amplification strategy has the following prominent advantages: (1) Photothermal-induced sensing interface regulation opened up a new avenue for electrochemical signal amplification by simple NIR light controlling to shorten the OHP, which proffered inspiration for the development of future electrochemical biosensors with high sensitivity. (2) An NIR-responsive hydrogel was utilized as a dual-mode signal probe with eminent loading capacity, further enhancing the electrochemical and temperature signals; thus, the obtained dual signals mutually validated each other to improve the accuracy of results. (3) It was reasonable to believe that the shrinkage behavior of the NIR-responsive hydrogel could become a promising candidate for signal modulation. Importantly, the success in the establishment of the electrochemical-interface-regulated immunoassay expanded the application of photothermal sensing and enriched the signal amplification strategy in clinical diagnosis.

■ ASSOCIATED CONTENT

Supporting Information

The Supporting Information is available free of charge at https://pubs.acs.org/doi/10.1021/acsabm.1c00665.

Materials and reagents; apparatus; optimization of experimental conditions; stability evaluation of the immunosensor; recovery measurements of HE4 in human serum samples; and comparison with various methods of HE4 detection (PDF)

■ AUTHOR INFORMATION

Corresponding Author

Hong Dai − *College of Chemistry and Materials, Fujian Normal University, Fuzhou, Fujian 350108, China;* orcid.org/0000-0001-8212-3474; Email: dhong@fjnu.edu.cn; Fax: (+86)-591-22866135

Authors

Shupei Zhang − *College of Chemistry and Materials, Fujian Normal University, Fuzhou, Fujian 350108, China; College of Chemical and Material Engineering, Quzhou University, Quzhou, Zhejiang 32400, China*

Huizhu Ren − *College of Chemistry and Materials, Fujian Normal University, Fuzhou, Fujian 350108, China*

Liang Lv − *College of Chemical and Material Engineering, Quzhou University, Quzhou, Zhejiang 32400, China*

Yanyu Lin − *College of Chemical and Material Engineering, Quzhou University, Quzhou, Zhejiang 32400, China*

Complete contact information is available at: https://pubs.acs.org/10.1021/acsabm.1c00665

Notes

The authors declare no competing financial interest.

■ ACKNOWLEDGMENTS

The authors gratefully acknowledge the financial support from the National Natural Science Foundation of China (21877012 and 21575024), the National Science Foundation of Fujian Province (2020J02034 and 2019J01052063), and the Health Education Joint Research Project of Fujian Province (2019-WJ-04).

■ REFERENCES

(1) Wang, L. Y.; Rong, Q. F.; Ma, Z. F. Construction of Electrochemical Immunosensing Interface for Multiple Cancer Biomarkers Detection. *Electroanalysis* **2016**, *28*, 1692−1699.

(2) Wilson, R. E.; O'Connor, R.; Gallops, C. E.; Kwizera, E. A.; Noroozi, B.; Morshed, B. I.; Wang, Y.; Huang, X. Immunomagnetic Capture and Multiplexed Surface Marker Detection of Circulating Tumor Cells with Magnetic Multicolor Surface-Enhanced Raman Scattering Nanotags. *ACS Appl. Mater. Interfaces* **2020**, *12*, 47220−47232.

(3) Muzyka, K. Current trends in the development of the electrochemiluminescent immunosensors. *Biosens. Bioelectron.* **2014**, *54*, 393−407.

(4) Biswas, S.; Lan, Q.; Xie, Y.; Sun, X.; Wang, Y. Label-Free Electrochemical Immunosensor for Ultrasensitive Detection of Carbohydrate Antigen 125 Based on Antibody-Immobilized Bio-

compatible MOF-808/CNT. *ACS Appl. Mater. Interfaces* **2021**, *13*, 3295−3302.
(5) Xu, D. D.; Liu, C.; Li, C. Y.; Song, C. Y.; Kang, Y. F.; Qi, C. B.; Lin, Y.; Pang, D. W.; Tang, H. W. Dual Amplification Fluorescence Assay for Alpha Fetal Protein Utilizing Immunohybridization Chain Reaction and Metal-Enhanced Fluorescence of Carbon Nanodots. *ACS Appl. Mater. Interfaces* **2017**, *9*, 37606−37614.
(6) Sun, Y.; Zhu, X.; Liu, H.; Dai, Y.; Han, R.; Gao, D.; Luo, C.; Wang, X.; Wei, Q. Novel Chemiluminescence Sensor for Thrombin Detection Based on Dual-Aptamer Biorecognition and Mesoporous Silica Encapsulated with Iron Porphyrin. *ACS Appl. Mater. Interfaces* **2020**, *12*, 5569−5577.
(7) Zhou, Y.; He, J.; Zhang, C.; Li, J.; Fu, X.; Mao, W.; Li, W.; Yu, C. Novel Ce(III)-Metal Organic Framework with a Luminescent Property To Fabricate an Electrochemiluminescence Immunosensor. *ACS Appl. Mater. Interfaces* **2020**, *12*, 338−346.
(8) Li, L.; Wang, T.; Zhang, Y.; Xu, C.; Zhang, L.; Cheng, X.; Liu, H.; Chen, X.; Yu, J. Editable TiO2 Nanomaterial-Modified Paper in Situ for Highly Efficient Detection of Carcinoembryonic Antigen by Photoelectrochemical Method. *ACS Appl. Mater. Interfaces* **2018**, *10*, 14594−14601.
(9) El-Moghazy, A. Y.; Huo, J.; Amaly, N.; Vasylieva, N.; Hammock, B. D.; Sun, G. An Innovative Nanobody-Based Electrochemical Immunosensor Using Decorated Nylon Nanofibers for Point-of-Care Monitoring of Human Exposure to Pyrethroid Insecticides. *ACS Appl. Mater. Interfaces* **2020**, *12*, 6159−6168.
(10) Li, Q.; Zeng, L.; Wang, J.; Tang, D.; Liu, B.; Chen, G.; Wei, M. Magnetic Mesoporous Organic−Inorganic NiCo2O4 Hybrid Nanomaterials for Electrochemical Immunosensors. *ACS Appl. Mater. Interfaces* **2011**, *3*, 1366−1373.
(11) Wu, L.; Hu, Y.; Sha, Y.; Li, W.; Yan, T.; Wang, S.; Li, X.; Guo, Z.; Zhou, J.; Su, X. An ″in-electrode″-type immunosensing strategy for the detection of squamous cell carcinoma antigen based on electrochemiluminescent AuNPs/g-C3N4 nanocomposites. *Talanta* **2016**, *160*, 247−255.
(12) Shao, H. L.; Lu, J.; Zhang, Q. Q.; Hu, Y. F.; Wang, S.; Guo, Z. Y. Ruthenium-based metal organic framework (Ru-MOF)-derived novel Faraday-cage electrochemiluminescence biosensor for ultrasensitive detection of miRNA-141. *Sens. Actuators, B* **2018**, *268*, 39−46.
(13) Guo, Z.; Sha, Y.; Hu, Y.; Wang, S. In-electrode vs. on-electrode: ultrasensitive Faraday cage-type electrochemiluminescence immunoassay. *Chem. Commun.* **2016**, *52*, 4621−4.
(14) Kannan, P.; Chen, J.; Su, F.; Guo, Z.; Huang, Y. Faraday-Cage-Type Electrochemiluminescence Immunoassay: A Rise of Advanced Biosensing Strategy. *Anal. Chem.* **2019**, *91*, 14792−14802.
(15) Lu, J.; Wu, L.; Hu, Y.; Wang, S.; Guo, Z. Ultrasensitive Faraday cage-type electrochemiluminescence assay for femtomolar miRNA-141 via graphene oxide and hybridization chain reaction-assisted cascade amplification. *Biosens. Bioelectron.* **2018**, *109*, 13−19.
(16) Xu, L.; Zhang, Q.; Hu, Y.; Ma, S.; Hu, D.; Wang, J.; Rao, J.; Guo, Z.; Wang, S.; Wu, D.; Liu, Q.; Peng, J. Ultrasensitive mushroom-like electrochemical immunosensor for probing the activity of histone acetyltransferase. *Anal. Chim. Acta* **2019**, *1066*, 28−35.
(17) Hu, Y.; Zhang, Q.; Hu, D.; Wang, J.; Rao, J.; Xu, L.; Guo, Z.; Wang, S.; Liu, X.; Tang, S.; Shen, Q. Ultrasensitive electrochemiluminescence immunosensor for the transcriptional co-activator p300 by using a graphene oxide monolayer and tetrahedral DNA-mediated signal amplification. *Microchim. Acta* **2019**, *186*, No. 325.
(18) Wang, T.; Song, X.; Lin, H.; Hao, T.; Hu, Y.; Wang, S.; Su, X.; Guo, Z. A Faraday cage-type immunosensor for dual-modal detection of Vibrio parahaemolyticus by electrochemiluminescence and anodic stripping voltammetry. *Anal. Chim. Acta* **2019**, *1062*, 124−130.
(19) Huang, K.; Wu, H.; Jiang, F.; Shen, G.; Wang, L. On the near-infrared light-responsive and mechanical properties of PNIPAM-based nanocomposite hydrogels. *Polym. Degrad. Stab.* **2018**, *156*, 228−233.
(20) Wei, Y.; Zeng, Q.; Wang, M.; Huang, J.; Guo, X.; Wang, L. Near-infrared light-responsive electrochemical protein imprinting biosensor based on a shape memory conducting hydrogel. *Biosens. Bioelectron.* **2019**, *131*, 156−162.
(21) Gao, N.; Gao, F.; He, S.; Zhu, Q.; Huang, J.; Tanaka, H.; Wang, Q. Graphene oxide directed in-situ deposition of electroactive silver nanoparticles and its electrochemical sensing application for DNA analysis. *Anal. Chim. Acta* **2017**, *951*, 58−67.
(22) Ran, X.; Du, Y.; Wang, Z.; Wang, H.; Pu, F.; Ren, J.; Qu, X. Hyaluronic Acid-Templated Ag Nanoparticles/Graphene Oxide Composites for Synergistic Therapy of Bacteria Infection. *ACS Appl. Mater. Interfaces* **2017**, *9*, 19717−19724.
(23) Pinaud, F.; Russo, L.; Pinet, S.; Gosse, I.; Ravaine, V.; Sojic, N. Enhanced electrogenerated chemiluminescence in thermoresponsive microgels. *J. Am. Chem. Soc.* **2013**, *135*, 5517−20.
(24) Sun, J.; Zhou, F.; Hu, H.; Li, N.; Xia, M.; Wang, L.; Wang, X.; Wang, G. Photocontrolled Thermosensitive Electrochemiluminescence Hydrogel for Isocarbophos Detection. *Anal. Chem.* **2020**, *92*, 6136−6143.
(25) Song, X.; Xv, L.; Wu, L.; Hu, Y.; Wang, S.; Guo, Z.; Su, X. Electrochemical Immunosensor for Detection of Vibrio parahaemolyticus Based on Faradaycage-Type Anodic Stripping Voltammetry. *J. Electrochem. Soc.* **2017**, *164*, B704−B709.
(26) Hong, Z.; Hong, J.; Xie, C.; Huang, Z.; Wei, M. Hierarchical rutile TiO2 with mesocrystalline structure for Li-ion and Na-ion storage. *Electrochim. Acta* **2016**, *202*, 203−208.
(27) Hummers, W. S.; Offeman, R. E. Preparation of Graphitic Oxide. *J. Am. Chem. Soc.* **1958**, *80*, 1339.
(28) Zhang, H.; Zhang, Q.; Zhang, L.; Pei, T.; Li, E.; Wang, H.; Zhang, Q.; Xia, L. Temperature-Responsive Electrocatalysis Based on Poly(N-Isopropylacrylamide)-Modified Graphene Oxide (PNIPAm-GO). *Chem. - Eur. J.* **2019**, *25*, 1535−1542.
(29) Qiao, P.; Sun, B.; Li, H.; Pan, K.; Tian, G.; Wang, L.; Zhou, W. Surface Plasmon Resonance-Enhanced Visible-NIR-Driven Photocatalytic and Photothermal Catalytic Performance by Ag/Mesoporous Black TiO2 Nanotube Heterojunctions. *Chem. - Asian J.* **2019**, *14*, 177−186.
(30) Huang, L.; Yang, H. T.; Zhang, Y. H.; Xiao, W. Study on Synthesis and Antibacterial Properties of Ag NPs/GO Nanocomposites. *J. Nanomater.* **2016**, *2016*, No. 5685967.

https://doi.org/10.1021/acsabm.1c00665
ACS Appl. Bio Mater. XXXX, XXX, XXX−XXX